Linearly forced isotropic turbulence

By T. S. Lundgren †

Stationary isotropic turbulence is often studied numerically by adding a forcing term to the Navier-Stokes equation. This is usually done for the purpose of achieving higher Reynolds number and longer statistics than is possible for isotropic decaying turbulence. It is generally accepted that forcing the Navier-Stokes equation at low wave number does not influence the small scale statistics of the flow provided that there is wide separation between the largest and smallest scales. It will be shown, however, that the spectral width of the forcing has a noticeable effect on *inertial range* statistics. A case will be made here for using a broader form of forcing in order to compare computed isotropic stationary turbulence with (decaying) grid turbulence. It is shown that using a forcing function which is directly proportional to the velocity has physical meaning and gives results which are closer to both homogeneous and non-homogeneous turbulence.

Section 1 presents a four part series of motivations for linear forcing. Section 2 puts linear forcing to a numerical test with a pseudospectral computation.

1. Motivation for Linear Forcing

1.1. *Linearity of energy production in non-homogeneous turbulence*

In shearflow turbulence the equation for the fluctuating part of the velocity, $\mathbf{u}'$, is

$$\frac{\partial \mathbf{u}'}{\partial t} + \overline{\mathbf{u}} \cdot \nabla \mathbf{u}' + \mathbf{u}' \cdot \nabla \overline{\mathbf{u}} + \mathbf{u}' \cdot \nabla \mathbf{u}' - \nabla \cdot \overline{\mathbf{u}'\mathbf{u}'} = -\nabla p'/\rho + \nu \nabla^2 \mathbf{u}'. \tag{1}$$

The third term on the left, $\mathbf{u}' \cdot \nabla \overline{\mathbf{u}}$ appears in the turbulent energy equation as the energy production term, $< \mathbf{u}' \cdot \nabla \overline{\mathbf{u}} \cdot \ \mathbf{u}' >$. (Both angle brackets and overbars are used to denote averages.) In (1) it appears as a forcing term proportional to $\mathbf{u}'$. This suggests that for isotropic homogeneous turbulence it might be appropriate to force a stationary flow with a driving term proportional to the velocity. Of course, for isotropic turbulence there is no mean velocity gradient, so the only way to have the flow be isotropic and stationary is to have the forcing be isotropic. It is proposed here to use

$$\frac{\partial \mathbf{u}}{\partial t} + \mathbf{u} \cdot \nabla \mathbf{u} = -\nabla p/\rho + \nu \nabla^2 \mathbf{u} + \mathbf{f} \tag{2}$$

with the driving force

$$\mathbf{f} = Q\mathbf{u} \ , \tag{3}$$

where Q is a constant. The prime on the velocity has been omitted here and henceforth with the understanding that $< \mathbf{u} >= 0$. The turbulent energy equation is now

$$\frac{1}{2} \frac{\partial < \mathbf{u} \cdot \mathbf{u} >}{\partial t} = -\epsilon + Q < \mathbf{u} \cdot \mathbf{u} >, \tag{4}$$

where

$$\epsilon = -\nu < \mathbf{u} \cdot \nabla^2 \mathbf{u} > \tag{5}$$

† University of Minnesota

is the mean dissipation rate and the last term could be called *isotropic turbulent production*. For *stationary* turbulence therefore (setting the time derivative to zero)

$$Q = \epsilon/3U^2 \tag{6}$$

where $U^2 =< \mathbf{u}\cdot\mathbf{u} > /3$ is the mean square of one component of the velocity. The proposal is to numerically solve

$$\frac{\partial \mathbf{u}}{\partial t} + \mathbf{u}\cdot\nabla\mathbf{u} = -\nabla p/\rho + \nu\nabla^2\mathbf{u} + (\epsilon/3U^2)\mathbf{u} \tag{7}$$

with the objective of comparing the statistics with those of grid flow turbulence. Equation (7) has the property that the rest state is unstable to long waves. Therefore solutions cannot decay to zero but must transfer energy to shorter waves in order to dissipate energy. Some reasons are given below for expecting computational results to be comparable with experiments for inertial scales of turbulence.

1.2. *Linear forcing of the Karman-Howarth equation*

A derivation of the Karman-Howarth equation, following the steps given in detail by Landau and Lifshitz (1959), but including a forcing term as in (2), gives

$$\frac{\partial U^2}{\partial t} - \frac{1}{2}\frac{\partial B_2}{\partial t} - \frac{1}{6}\frac{1}{r^4}\frac{\partial}{\partial r}r^4 B_3 =$$

$$-\nu\frac{1}{r^4}\frac{\partial}{\partial r}r^4\frac{\partial B_2}{\partial r} + \frac{1}{r^3}\int_0^r r^2 < \mathbf{u}(\mathbf{x_2},t)\cdot\mathbf{f}(\mathbf{x_1},t) + \mathbf{u}(\mathbf{x_1},t)\cdot\mathbf{f}(\mathbf{x_2},t) > dr \tag{8}$$

where $B_2(r,t)$ and $B_3(r,t)$ are second and third order longitudinal structure functions, $\mathbf{x}_2 = \mathbf{x}_1 + \mathbf{r}$ and $r = |\mathbf{r}|$. With $\mathbf{f}$ given by (3), the last term can be written

$$\frac{1}{r^3}\int_0^r 2Qr^2 R_{ii}(r,t)dr \tag{9}$$

where $R_{ij}(r,t) =< u_i(\mathbf{x}_1,t)u_j(\mathbf{x}_1+\mathbf{r},t) >$ is the velocity correlation tensor. Since the trace of the correlation tensor is related to the second order structure function by

$$R_{ii} = 3U^2 - \frac{1}{2r^2}\frac{\partial}{\partial r}r^3 B_2 \tag{10}$$

(9) can be integrated to the form

$$2QU^2 - QB_2(r,t)\ . \tag{11}$$

Using this with Q given by (6), and dropping the time derivatives for stationary turbulence, gives the result

$$-\frac{2}{3}\epsilon + \frac{\epsilon}{3U^2}B_2 = \frac{1}{6r^4}\frac{\partial}{\partial r}r^4 B_3 - \nu\frac{1}{r^4}\frac{\partial}{\partial r}r^4\frac{\partial B_2}{\partial r} \tag{12}$$

in which ϵ is a constant given by (5). This differs from the standard decaying version of the Karman-Howarth equation which is

$$-\frac{2}{3}\epsilon - \frac{1}{2}\frac{\partial B_2}{\partial t} = \frac{1}{6}\frac{1}{r^4}\frac{\partial}{\partial r}r^4 B_3 - \nu\frac{1}{r^4}\frac{\partial}{\partial r}r^4\frac{\partial B_2}{\partial r} \tag{13}$$

where here ϵ is a function of *time* given by

$$\epsilon(t) = -\frac{3}{2}\frac{dU^2}{dt} \equiv \frac{15\nu}{2}\frac{d^2B_2}{dr^2}\Big|_0\ . \tag{14}$$

The Kolmogorov $r^{2/3}$ law may be derived from (12), by the method of matched asymptotic expansions, in a manner similar to that employed by Lundgren (2002) to get that law from (13) but without the necessity of using similarity in time. The result is the same:

$$B_2 = C_2 U^2 (r/L)^{2/3} \equiv C_2(\epsilon r)^{2/3} \tag{15}$$

where $L = U^3/\epsilon$ and ϵ and U^2 are independent of time now.

Equation(12) can be integrated to obtain B_3 in terms of B_2, as

$$B_3 = 6\nu \frac{\partial B_2}{\partial r} - \frac{4}{5}\epsilon r + \frac{2\epsilon}{U^2}\frac{1}{r^4}\int_0^r r^4 B_2 dr \quad . \tag{16}$$

Using (15) for B_2 gives the simple result

$$\frac{B_3}{U^3} = \frac{4C_2}{R_L}\Big(\frac{r}{L}\Big)^{-1/3} - \frac{4}{5}\Big(\frac{r}{L}\Big) + \frac{6C_2}{17}\Big(\frac{r}{L}\Big)^{5/3} \quad . \tag{17}$$

This may be rewritten using the Taylor microscale λ to scale r:

$$B_3 = -\frac{4}{5}\epsilon r\left(1 - R_\lambda^{-2/3}\left(2.678C_2\Big(\frac{r}{\lambda}\Big)^{2/3} + 2.029C_2\Big(\frac{r}{\lambda}\Big)^{-4/3}\right)\right) \tag{18}$$

Here $R_L = UL/\nu$; $R_L = R_\lambda^2/15$ relates R_λ and R_L and $\lambda/L = 15/R_\lambda$ relates λ and L. The corresponding result for decaying turbulence (Lundgren 2002; Lindborg 1999) is almost the same:

$$B_3 = -\frac{4}{5}\epsilon r\left(1 - R_\lambda^{-2/3}\left(2.678\Big(\frac{2}{3}\ \frac{1+n}{n}\Big)C_2\Big(\frac{r}{\lambda}\Big)^{2/3} + 2.029C_2\Big(\frac{r}{\lambda}\Big)^{-4/3}\right)\right) \tag{19}$$

where n is the energy decay exponent ($U^2 \propto t^{-n}$). Equations (18) and (19) would be exactly the same if $n = 2$, which is not a realistic decay exponent; $n = 1.2$ is often observed and $n = 4/3$ is the maximum value possible. These equations give a Reynolds number correction to the Kolmogorov "4/5" law showing that it is approached slowly as $R_\lambda \to \infty$. When $C_2 = 2$ and $n = 1.2$ the compensated forms have maxima at $r/\lambda = 1.23$ (for linearly forced turbulence) and $r/\lambda = 1.11$ (for decaying turbulence).

The similarity of these equations can be seen in Figure 1 where they are plotted for $R_\lambda = 350$ and compared with an experiment in a turbulent jet.

1.3. *Normalized decaying turbulence*

Consider (7) again, with and without the isotropic forcing term. In the stationary case with forcing introduce dimensionless variables

$$\mathbf{v} = \mathbf{u}/U, \quad \mathbf{x} = \mathbf{r}/L, \quad \tau = tU/L \tag{20}$$

where U and $L = U^3/\epsilon$ are constants. A simple change of variables gives

$$\frac{\partial \mathbf{v}}{\partial \tau} + \mathbf{v}\cdot\nabla\mathbf{v} = -\nabla P + R_L^{-1}\nabla^2\mathbf{u} + \frac{1}{3}\mathbf{v} \quad . \tag{21}$$

Now consider the case without the forcing term, with the change of variables

$$\mathbf{v} = \mathbf{u}/U(t), \quad \mathbf{x} = \mathbf{r}/L(t), \quad \tau = \int_0^t U/L\ dt \tag{22}$$

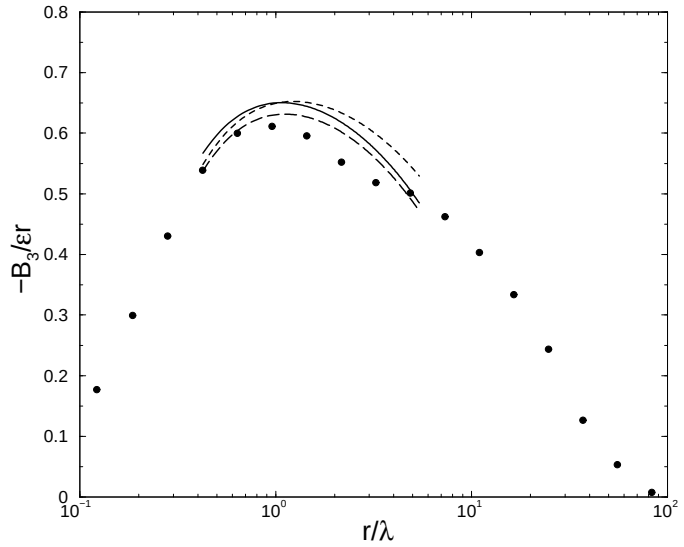

Figure 1. Compensated third order structure function vs. r/λ at $R_\lambda = 350$. The data points are from a laboratory jet (Gagne, 2002) at the same value of R_λ. The long dashed curve is from (19). The dashed curve is the linear forcing result from (18). The solid line is from the computation of section 2 using the $R_\lambda^{-2/3}$ scaling law to extrapolate from $R_\lambda = 170$ to $R_\lambda = 350$.

The equation transforms to

$$\frac{\partial \mathbf{v}}{\partial \tau} + \mathbf{v}\cdot\nabla\mathbf{v} = -\nabla P + R_L^{-1}\nabla^2\mathbf{v} - \frac{L\dot{U}}{U^2}\mathbf{v} + \frac{\dot{L}}{U}\mathbf{x}\cdot\nabla\mathbf{v}. \tag{23}$$

Using $\epsilon = -\frac{3}{2}\frac{dU^2}{dt}$ and $L = U^3/\epsilon$ the coefficient of $\mathbf{v}$ is $-\frac{1}{3}$, so

$$\frac{\partial \mathbf{v}}{\partial \tau} + \mathbf{v}\cdot\nabla\mathbf{v} = -\nabla P + R_L^{-1}\nabla^2\mathbf{v} + \frac{1}{3}\mathbf{v} \quad + \frac{\dot{L}}{U}\mathbf{x}\cdot\nabla\mathbf{v}\ . \tag{24}$$

While this is not exactly the same as (21) because of the last term, it is apparent that energy decay has the effect of an isotropic forcing term. Note also that if $U^2 \propto t^{-n}$ then $\epsilon \propto t^{-n-1}$ and $L = U^3/\epsilon \propto t^{1-n/2}$. So $\dot{L}$ would be zero if $n = 2$. In this case the equations would be the same except for the time dependence of R_L.

1.4. *Comparison with low wavenumber forcing*

In this subsection a more general forcing function is applied to the Karman-Howarth equation in order to show that the forcing range has a significant effect on the third order compensated structure function and presumably on any inertial range statistics. This analysis is carried out in detail in Appendix I and only summarized here. A Gaussian filter is applied to the velocity field, filtering out a variable part of the high wavenumber content. This filtered velocity is used as a forcing function for the Karman-Howarth equation. In one limit there is uniform linear forcing. The results of a calculation are shown in Figure 2a for different values of KL. Here K is the width of the filter; wavenumbers greater than K are filtered out. When K is small only low wavenumbers are forced, while if $K \to \infty$ forcing is uniform over all wavenumbers. The figure shows the compensated

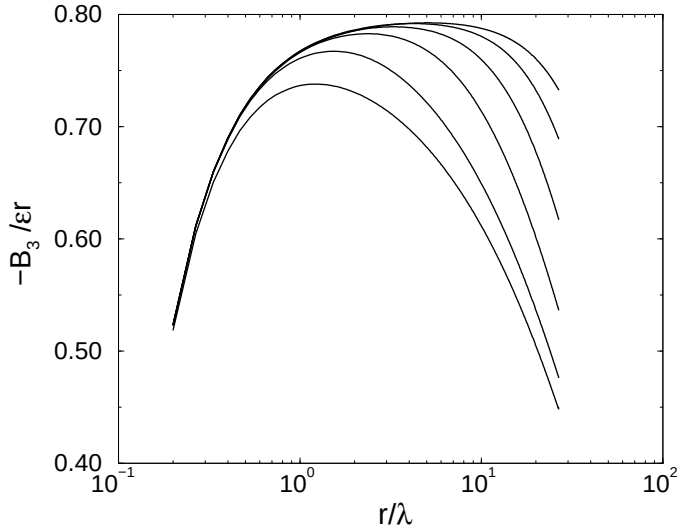

Figure 2a. Third order compensated structure functions for variations of the forcing range computed from (A17). The curves are (from the bottom) for $KL = 1000, 100, 25, 10, 5, 3$. The lowest curve ($KL = 1000$) is close to the linear forcing result from (18). All the curves are computed for $R_\lambda = 1000$.

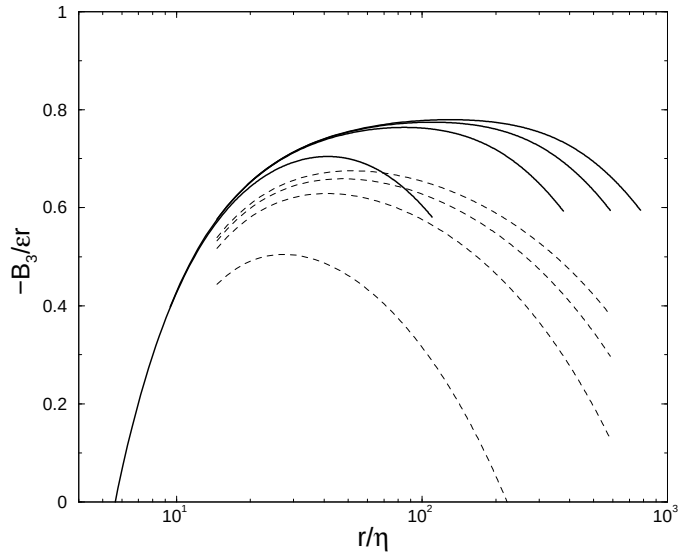

Figure 2b. Solid curves, third order compensated structure function vs. r/η for $KL = 5$ and $R_\lambda = 125, 284, 381, 460$ from the bottom up. This compares with the low wavenumber forced computation of Gotoh et. al. (2002) at the same Reynolds numbers (compare their Fig.12). The maximum values shift to the right and increase with increasing R_λ in a similar manner. The maxima are .70, .76, .77, .78 comparing with .66, .77, .78, .76 from Gotoh. The dashed curves are for linear forcing at the same values of R_λ from (18) showing the differences.

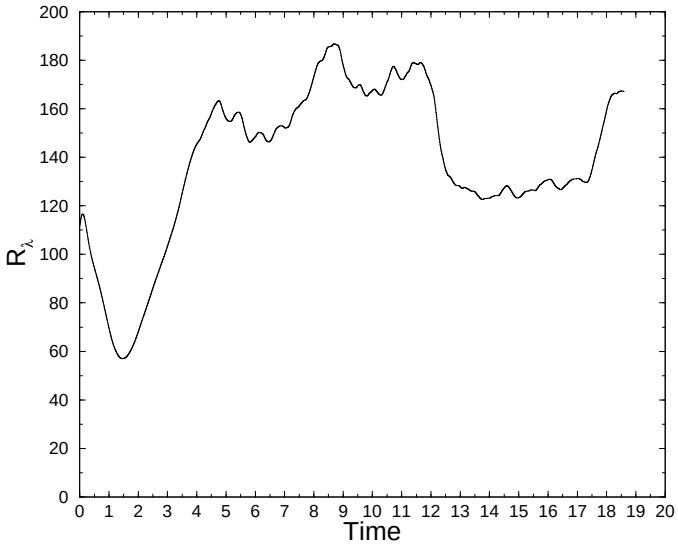

Figure 3. Time History of R_λ with linear forcing. Numerical data for the following figures was taken over a time range of about .5 near T=10, where $R_\lambda = 170$.

third order structure function for different values of KL for $R_\lambda = 1000$. When $KL = 1000$ the curve is nearly the same as computed from (18). As KL decreases the maximum value moves to the right and increases towards 4/5, greatly distorting the structure function in the inertial range.

Figure 2b shows compensated structure functions for several values of R_λ for the single value $KL = 5$. This was constructed in order to compare with the high resolution DNS of Gotoh et. al. (2002), which was driven by white noise in a low wavenumber band which corresponds roughly to a Gaussian filter with width $KL = 5$. (In their numerics at $R_\lambda = 460$ $L \sim 2.5$, making $K = 2$ which is in approximate accord with their forcing range of $1 < k < \sqrt{6}$.)

2. Pseudospectral Computation with Linear Forcing

Computations have been carried out with a Rogallo/Wray pseudospectral code, modified slightly to accomodate linear forcing. This was done with $(256)^3$ resolution with $\nu = .003$, box size 2π on a side, and time scale set by taking $Q = 1$. Figure 3 shows the time history of R_λ during a lengthy run. As can be seen the computation is not exactly stationary (but should be statistically stationary after an initial transient). The instantaneous value of $\epsilon/3U^2$ (not shown here) fluctuates about unity by about $\pm 20\%$. There are fairly stationary periods, however. Data for the following figures was taken in a relatively stationary period near $T = 10$ where $R_\lambda = 170$.

Figure 4 shows the energy spectrum versus $k\eta$. The spectrum is a little shallower than $k^{-5/3}$ (the upper straight line on the figure). Mydlarski and Warhaft (1996) indicate approximately $k^{-1.45}$ at this Reynolds number for grid flow turbulence.

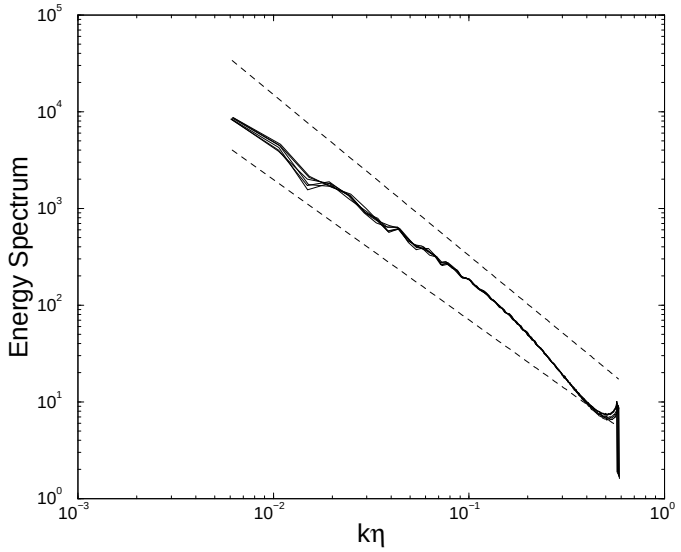

Figure 4. Energy spectrum in Kolmogorov variables for $R_\lambda = 170$. The upper straight line is $k^{-5/3}$ and the lower one is $k^{-1.45}$.

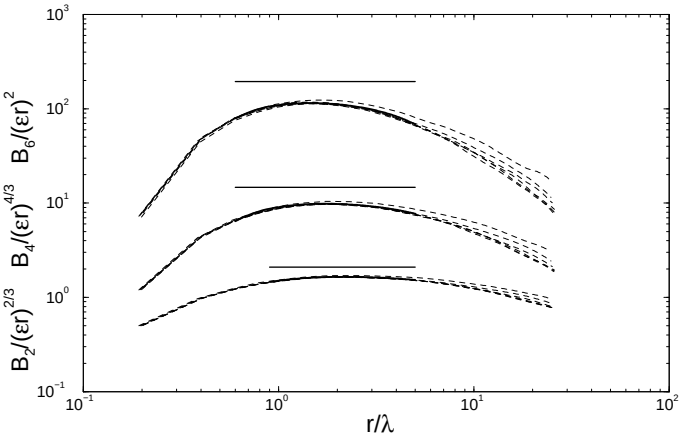

Figure 5. Compensated even order structure functions versus r/λ for $R_\lambda = 170$. Solid lines are curve fit using (25). The solid straight lines are an extrapolation to $R_\lambda = \infty$ using V_2, V_4, V_6.

In Figure 5 compensated structure functions of second, fourth, and sixth order are plotted versus r/λ. The minimum separation between two points ($2\pi/256$) is very nearly $.2\lambda$. The output was taken by averaging over all pairs of points along the x direction with separation r (which is a multiple of $.2\lambda$). For each structure function there are six curves (the lighter long-dashed curves on the figure), one each for times separated by 1000 time steps. The total elapsed time for 5000 time steps is about .5 time units on Figure 3. The spread of these curves indicates the random nature of the output even after the spatial averaging.

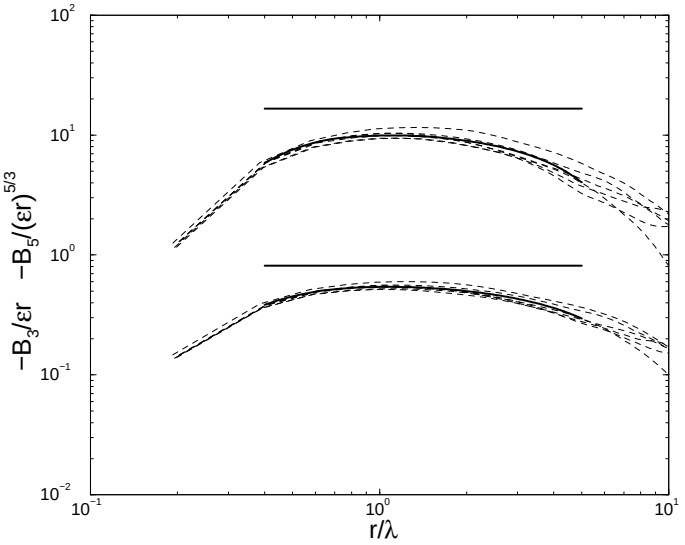

Figure 6. Odd order compensated structure functions for $R_\lambda = 170$. Curve fit same as in Figure 5.

The *pth* order compensated structure function should take the form (Lundgren 2003)

$$B_p/(\epsilon r)^{p/3} = V_p\Big(1 - R_\lambda^{-2/3}\big(A_p(r/\lambda)^{2/3} + B_p(r/\lambda)^{-4/3}\big)\Big) \quad . \tag{25}$$

This gives Reynolds number corrections to Kolmogorov (1941) theory and can be regarded as a scaling law. If the parameters V_p, A_p, B_p were determined for some Reynolds number (numerically or by experiment) one could extrapolate the data to another Reynolds number. The coefficients for $p = 2, 3, 4, 5, 6$ were determined as follows. The six time sets were truncated to about $.5 < r/\lambda < 5$ in order to get the upper parts of the sets, roughly centered about the maxima. These were accumulated into into a single set, which looks like a lot of scattered experimental points. Then using a nonlinear curve fitting algorithm (on xmgr) the coefficients V_p, A_p, B_p were determined for $R_\lambda = 170$ ($R_\lambda^{-2/3} = .033$). The values are shown in the table below.

p	V_p	A_p	B_p	$(r/\lambda)_{\max}$	$V_p/p!$
2	2.11	2.62	6.15	2.17	1.05
3	−.824	6.56	3.75	1.07	−.137
4	15.24	4.85	7.65	1.78	.635
5	−16.91	7.81	4.53	1.08	−.141
6	197.5	6.56	6.87	1.45	.274

Table 1. Coefficients for (25). Fifth column is position of maximum of $B_3/\epsilon r$. Sixth column compares V_p with $p!$.

The fit curves are shown as heavy lines which approximate the data fairly well. These should be thought of as time averages of the six curves of each set. The horizontal straight lines above each set are the curves $B_p/(\epsilon r)^{p/3} = V_p$, representing an extrapolation to

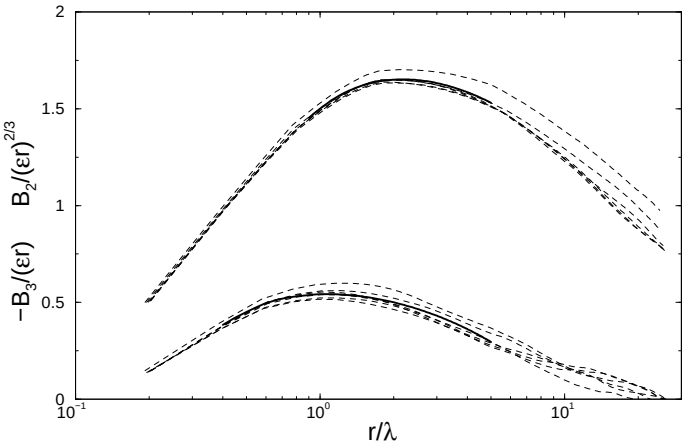

Figure 7. Second and third order structure functions repeated from figures 5 and 6 on a semilog plot in order to better show the nature of the curve fit.

$R_\lambda = \infty$. In particular note that the horizontal line above the second order stucture function, $V_2 = 2.11$, is an acceptable value for that asymptote.

The third and fifth order structure functions were treated in the same way and shown in Figure 6. The individual sets show much more scatter than the even order structure functions because of cancellation between the left and right sides of the almost symmetric pdfs. Note the value $V_3 = .824$. This should be exactly .8, the Kolmogorov "4/5" law. Figure 7 repeats the B_2 and B_3 curves from Figures 5 and 6 on a semilog plot.

The maxima of the compensated structure functions have positions which scale with λ. For even orders the positions shift towards smaller values with increasing order. For odd orders there is not much shift. The rapid increase of the magnitude of the even orders with increasing order required that they be presented on a log-log plot in order to show them on the same figure. A rapid increase of moments like $p!$, as seen in the table, is a signature for exponential tails on the pdf. This is observed approximately in Figure 8.

An example of extrapolation for the third order structure function is shown in Figure 1, where the curve fit values of V_3, A_3, B_3 are used to extrapolate to $R_\lambda = 350$ ($R_\lambda^{-2/3} = .020$).

Figure 8 is the final figure. This shows the velocity pdf versus v/σ where v is the velocity difference between two points along the x direction and σ is the standard deviation, $\sigma =< v^2 >^{1/2}$. In these variables the average and the second moment are both unity. The outermost curve is as close to the pdf of the velocity derivative as can be reached with this resolution. The fluctuations in the tails were ameliorated to some extent by accumulating the pdfs over 10 successive time steps (in addition to spatial averaging).

3. Conclusions

There were two objectives to this research. The first was to show that it is desirable and useful to compute stationary isotropic turbulence with a forcing function which is a simple linear function of velocity, which thus forces uniformly at all wavenumbers. This was done by analysis of of a forced Karman-Howarth equation, which allows calculation of third order structure functions in terms of second order structure functions. This allowed a

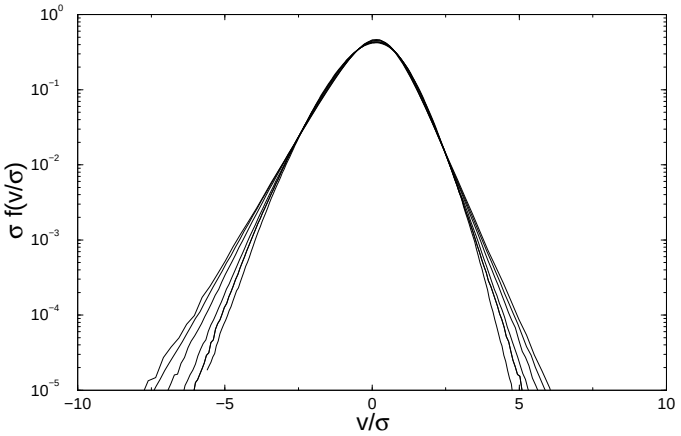

Figure 8. pdf of velocity difference vs. $v/\sigma, \sigma = < v^2 >^{1/2}$ The curves are for values of the separation. From the outside $r/\lambda = 2., .4, .6, 1.0, 1.4, 2.0, 2.4$

favorable comparison between decaying isotropic turbulence and linearly forced isotropic turbulence in subsection 1.2.

By applying filtered linear forcing to the Karman-Howarth equation it was shown that forcing at low wavenumber has a large effect on third-order structure functions, and would very likely influence all inertial range statistics, in partcular it could affect the computation of anomalous exponents. The third order structure function with low wavenumber filtered forcing was compared with high quality DNS (Gotoh et. al., 2002) and linear forcing was compared with experiments of Gagne (2002). The differences between low wave number forcing and linear forcing were considerable, as seen in Figure 2b, with low wavenumber forcing approaching the four-fifths law too rapidly with increasing Reynolds number.

The second objective was to compute a moderate resolution DNS of box turbulence with linear forcing to show the feasibility of such a computation. This was done in section 2. Compensated structure functions of second through sixth order were computed at $R_\lambda = 170$. It was shown that these could be fit with an $R_\lambda^{-2/3}$ scaling law, determining the coefficients to fit equation (25). (The analysis which produced this law (Lundgren 2003) applies equally to the forced Navier-Stokes equation.) The usefulness of the scaling law was demonstrated in Figure 1, where the third-order structure function computed at $R_\lambda = 170$ was extrapolated to $R_\lambda = 350$ (the solid curve in Figure 8 was extrapolated to the solid curve in Figure 1), where it compares with the Karman-Howarth results and with experiment.

4. ACKNOWLEDGEMENTS

The author would like to thank Bob Rogallo and Alan Wray for the use of their pseudospectral code, and Alan Wray and Nagi Mansour for help with the code and for helpful discussions during the work. Dale Pullin provided some much appreciated early encouragement.

5. Appendix I. Filtered Forcing.

With a general forcing term, the integrated Karman-Howarth equation is

$$B_3 = 6\nu\frac{dB_2}{dr} - \frac{4}{5}\epsilon r - \frac{6}{r^4}\int_0^r rdr\int_0^r < \mathbf{u}_2\cdot\mathbf{f}_1 + \mathbf{u}_1\cdot\mathbf{f}_2 > r^2 dr \quad . \tag{A1}$$

It is desired to develop a general case which includes forcing at small wavenumbers and also broader forcing. A simple model takes the forcing function proportional to the velocity, but with a variable part of the high wavenumber end filtered out with a Gaussian filter. A filtered velocity in Fourier space may be written

$$\tilde{\mathbf{u}}^<(\mathbf{k}) = \tilde{g}_K(k)\tilde{\mathbf{u}}(\mathbf{k}) \tag{A2}$$

where the filter and its transform are

$$g_K(x) = \int \exp(i\mathbf{k}\cdot\mathbf{x})\tilde{g}_K(k)d\mathbf{k} \tag{A3}$$

$$\tilde{g}_K(k) = \frac{1}{(2\pi)^3}\int \exp(-i\mathbf{k}\cdot\mathbf{x})g_K(x)d\mathbf{x} \tag{A4}$$

It is assumed that $\tilde{g}_K(0) = 1$ so that

$$\int g_K(x)d\mathbf{x} = (2\pi)^3 \quad . \tag{A5}$$

For a Gaussian filter

$$\tilde{g}_K = \exp(-.5k^2/K^2) \quad . \tag{A6}$$

This filters out wavenumbers $k > K$ for $0 < K < \infty$; $K = \infty$ is the uniform forcing case. The transform of $\tilde{g}_K$ is

$$g_K(x) = (2\pi)^{3/2}K^3\exp(-K^2x^2/2) \quad . \tag{A7}$$

In general the filtered physical space velocity is given by a convolution:

$$\mathbf{u}^<(\tilde{\mathbf{x}}) = \frac{1}{(2\pi)^3}\int g_K(|\mathbf{x}-\mathbf{s}|)\mathbf{u}(\mathbf{s})d\mathbf{s} \quad . \tag{A8}$$

The forcing function will be assumed to be $\mathbf{f} = Q\tilde{\mathbf{u}}^<$, where, since $\epsilon =< \mathbf{u}\cdot\mathbf{f} >$

$$Q = \epsilon/ < \mathbf{u}\cdot\tilde{\mathbf{u}}^< > \quad . \tag{A9}$$

From (A8)

$$< \mathbf{u}\cdot\mathbf{u}^< >= \frac{1}{(2\pi)^3}\int g_K(|\mathbf{x}-\mathbf{s}|) < \mathbf{u}(\mathbf{s})\cdot\mathbf{u}(\mathbf{x}) > d\mathbf{s} \tag{A10}$$

where

$$< \mathbf{u}(\mathbf{s})\cdot\mathbf{u}(\mathbf{x}) >= R_{ii}(|\mathbf{x}-\mathbf{s}|) \tag{A11}$$

is the trace of the correlation function given by (10). By using (A9) and (A10) the force correlation in (A1) may be written

$$< \mathbf{u}_2\cdot\mathbf{f}_1 + \mathbf{u}_1\cdot\mathbf{f}_2 >= 2\epsilon\frac{\int g_K(|\mathbf{x}-\mathbf{s}|)R_{ii}(s)d\mathbf{s}}{\int g_K(s)R_{ii}(s)d\mathbf{s}} \quad . \tag{A12}$$

Substituting this into (A1) gives

$$B_3 = 6\nu\frac{dB_2}{dr} -$$

$$\frac{\frac{4}{5}\epsilon r(2\pi)^3 3U^2 + \frac{12\epsilon}{r^4}\int_0^r rdr\int_0^r r^2dr\int g_K(|\mathbf{s}-\mathbf{r}|)\big(-\frac{1}{2}\frac{1}{s^2}\frac{d}{ds}s^3B_2(s)\big)d\mathbf{s}}{(2\pi)^3 3U^2 + \int g_K(s)\big(-\frac{1}{2}\frac{1}{s^2}\frac{d}{ds}s^3B_2(s)\big)d\mathbf{s}} \tag{A13}$$

where the integration over the $3U^2$ part of R_{ii} was done using (A5) and $\int_0^r rdr\int_0^r r^2dr = r^5/15$. In the upper integral do the integration over the angle variables with the Gaussian filter, obtaining

$$\int g_K(|\mathbf{s}-\mathbf{r}|)\sin(\theta)d\theta d\phi = (2\pi)^{5/2}KB(s,r) \tag{A14}$$

where

$$B(s,r) = \left(\frac{\big(\exp(-.5K^2(s-r)^2) - \exp(-.5K^2(s+r)^2)\big)}{sr}\right) \tag{A15}$$

is a temporary notation. Now do the integration by parts on s, which shifts the differentiation onto $B(s,r)$. The following identity may be proved

$$\frac{\partial B(s,r)}{\partial s} = \frac{1}{K^2s^2r^2}\frac{\partial A(s,r)}{\partial r} \tag{A16}$$

where

$$A(s,r) = (1-K^2sr)\exp(-.5K^2(s-r)^2) - (1+K^2sr)\exp(-.5K^2(s+r)^2) \quad .$$

Because of the $1/r^2$ factor in (A16) the inner $\int r^2dr$ may be carried out, resulting in the near-final form

$$\frac{B_3}{\epsilon r} = \frac{6L^2}{R_L}\frac{db_2}{dr} - \frac{\frac{4}{5} + (2\pi)^{-1/2}K^{-1}\frac{2}{r^5}\int_0^r rdr\int_0^\infty A(s,r)b_2(s)sds}{1-(2\pi)^{-1/2}K^5\frac{1}{3}\int_0^\infty \exp(-.5K^2s^2)b_2(s)s^4ds} \tag{A17}$$

where $b_2 = B_2/U^2$. The double integrals have to be integrated numerically with an assumed function for B_2. An appropriate form is

$$B_2 = 2U^2\tanh(.5C_2(r/L)^{2/3}) \tag{A18}$$

which gives the Kolmogorov two-thirds law for small r/L and tends to the proper limit $2U^2$ as $r/L \to \infty$.

REFERENCES

Gagne, Y. 2002 Private communication. The data were reported in the Ph.D. Thesis of Yann Malecot (1998, U. Grenoble).

Gotoh, T., Fukayama, D.& Nakano, T. 2002 Velocity field statistics in homogeneous steady turbulence obtained using a high resolution direct numerical simulation. *Phys. Fluids* **14**, 1065–1081.

von Karman, T. & Howarth, L. 1938 On the statistical theory of isotropic turbulence, *Proc. Roy. Soc. Lond.* A **164**, 192–215.

Kolmogorov, A. N. 1941 The local structure of turbulence in incompressible viscous fluid for very large Reynolds numbers, *Dokl. Akad. Nauk.*, SSSR **30**, 299-303. Reprinted in *Proc. Roy. Soc. London* A **434**, 9-13 (1991).

Landau, L. D. & Lifshitz, E. M. 1959 *Fluid Mechanics* Pergamon, London.

Lindborg, E. 1999 Correction to the four-fifths law due to variations of the dissipation, *Phys. Fluids* **11**, 510–512.

Lundgren, T. S. 2002 Kolmogorov two-thirds law by matched asymptotic expansion, *Phys. Fluids*, **14**, 638-642.

Lundgren, T. S. 2003 Kolmogorov turbulence by matched asymptotic expansion. *Phys. Fluids*, **15**, 1074–1081.

Mydlarski, L. & Warhaft, Z. 1996 On the onset of high-Reynolds-number grid-generated wind tunnel turbulence. *J. Fluid Mech.*, **320**, 331–368.